Biomech Model Mechanobiol (2013) 12:95–109
DOI 10.1007/s10237-012-0384-9

ORIGINAL PAPER

Microdomain heterogeneity in 3D affects the mechanics of neonatal cardiac myocyte contraction

Matthew W. Curtis · Elisa Budyn · Tejal A. Desai · Allen M. Samarel · Brenda Russell

Received: 31 August 2011 / Accepted: 23 February 2012 / Published online: 11 March 2012

Abstract Cardiac muscle cells are known to adapt to their physical surroundings, optimizing intracellular organization and contractile function for a given culture environment. A previously developed in vitro model system has shown that the inclusion of discrete microscale domains (or *microrods*) in three dimensions (3D) can alter long-term growth responses of neonatal ventricular myocytes. The aim of this work was to understand how cellular contact with such a domain affects various mechanical changes involved in cardiac muscle cell remodeling. Myocytes were maintained in 3D gels over 5 days in the presence or absence of $100-\mu$m-long microrods, and the effect of this local heterogeneity on cell behavior was analyzed via several imaging techniques. Microrod abutment resulted in approximately twofold increases in the maximum displacement of spontaneously beating myocytes, as based on confocal microscopy scans of the gel xy-plane or the myocyte long axis. In addition, microrods caused significant increases in the proportion of aligned myofibrils ($\leq 20°$ deviation from long axis) in fixed myocytes. Microrod-related differences in axial contraction could be abrogated by long-term interruption of certain signals of the RhoA-/Rho-associated kinase (ROCK) or protein kinase C (PKC) pathway. Furthermore, microrod-induced increases in myocyte size and protein content were prevented by ROCK inhibition. In all, the data suggest that microdomain heterogeneity in 3D appears to promote the development of axially aligned contractile machinery in muscle cells, an observation that may have relevance to a number of cardiac tissue engineering interventions.

Keywords Mechanobiology · Muscle hypertrophy · Digital image correlation · Microenvironment · Finite element · Mechanotransduction

Abbreviations

3D	Three dimensions
AraC	Cytosine β-D-arabino-furanoside
BSA	Bovine serum albumin
DAPI	4′,6-Diamidino-2-phenylindole
DMEM	Dulbecco's modified Eagle's medium
DMSO	Dimethyl sulfoxide
ECL	Enhanced chemiluminescence
ECM	Extracellular matrix
GAPDH	Glyceraldehyde-3-phosphate dehydrogenase
HRP	Horseradish peroxidase
MLC	Myosin light chain
MLCK	Myosin light chain kinase
MLCP	Myosin light chain phosphatase
PBS	Phosphate-buffered saline
PKC	Protein kinase C
PVDF	Polyvinylidene fluoride
RACK1	Receptor for activated C-kinase-1
ROCK	Rho-associated kinase

Electronic supplementary material The online version of this article (doi:10.1007/s10237-012-0384-9) contains supplementary material, which is available to authorized users.

M. W. Curtis · B. Russell (✉)
Department of Physiology and Biophysics, University of Illinois at Chicago, 835 South Wolcott Avenue, Chicago, IL 60612, USA
e-mail: russell@uic.edu

E. Budyn
Department of Mechanical and Industrial Engineering, University of Illinois at Chicago, Chicago, IL, USA

T. A. Desai
Department of Physiology and Division of Bioengineering, University of California at San Francisco, San Francisco, CA, USA

A. M. Samarel
The Cardiovascular Institute, Loyola University Medical Center, Maywood, IL, USA

SEM	Standard error of measurement
TBST	Tris-buffered saline-Tween 20

1 Introduction

Many cell types are known to be influenced by aspects of their physical environment, be it the varied extracellular architecture found in vivo or properties of a supporting substrate in vitro (Pedersen and Swartz 2005; Liu and Chen 2007). Isolated ventricular myocytes have been shown to respond to changes in substrate topography, geometry, rigidity, and strain (Simpson et al. 1999; Gopalan et al. 2003; Motlagh et al. 2003b; Engler et al. 2008; Jacot et al. 2008). Yet as tension-generating contractile cells, cardiac myocytes have the specialized ability to recognize such physical stimuli as they develop and transmit large intracellular forces. Cardiac myocytes balance extrinsic and intrinsic mechanics by activating processes of cell growth and myofibrillar or sarcomeric organization, which may serve to overcome an extremely limited proliferative potential (Soonpaa et al. 1996; Eble et al. 1998; Evans et al. 2003; Tiburcy et al. 2011). The result is a micromechanical integration of forces that determines the extent of myocyte adaptation.

Many of the pathways involved in the recognition of a physical stimulus by a cardiac myocyte have at least some dependence on outside-in signaling cascades. Through integrin-based points of contact with the extracellular milieu, cues are transduced by the actin cytoskeleton-linking protein complexes (Ross and Borg 2001; Samarel 2005). Indeed, the induction of myocyte hypertrophy can be specifically attributed to anchorage-dependent signaling molecules such as focal adhesion kinase (FAK), RhoA GTPase, and protein kinase C (PKC) (Sharp et al. 1997; Frey and Olson 2003; Hartman et al. 2009; Miyamoto et al. 2010). These proteins facilitate the changes in actin dynamics and focal adhesion assembly that are inherent to myofibrillar remodeling in vitro (Torsoni et al. 2005; DiMichele et al. 2009; Otani et al. 2011). Rho-associated kinase (ROCK), a target of GTP-bound RhoA, directly regulates several effectors including myosin light chain (MLC, also independently activated by myosin light chain kinase, MLCK), which leads to stress fiber formation and nonmuscle myosin-based cell contraction (Ren and Fang 2005).

The impact of engineered environments on the mechanobiological development of individual cardiac myocytes has not always been considered in tissue engineering approaches. A single myocyte can detect cell-scaled discontinuities in three dimensions (3D), reinforcing the need to understand muscle cell responses as a function of local cues (Curtis et al. 2010). Such cues were presented to myocytes as 100 − μm-long rigid polymeric structures (known as *microrods*) seeded with random orientation in a soft extracellular matrix (ECM) protein-rich gel. After 10 days in 3D culture, microrods led to increases in myocyte size and protein content that were similar to those caused by a potent chemical stimulus of hypertrophy, phenylephrine (Curtis et al. 2010). Microrod-interacting myocytes were also found to exhibit greater cross-sectional areas, rates of spontaneous contraction, and expression of muscle-regulating genes such as sarcoplasmic reticulum calcium-ATPase (SERCA2) and cardiac ankyrin repeat protein (CARP) (Curtis et al. 2010).

The current work uses this same method of culturing cells and microrods, but with the goal to understand how heterogeneity in 3D affects the mechanics of cardiac myocyte contraction. Techniques to analyze the contractile motion of myocytes generally require a measure of cellular displacement through tools such as marker beads or elastic pillars (Qin et al. 2007; Zhao et al. 2007; Kajzar et al. 2008). Other approaches gather displacements based on actual cell morphologies (Okada et al. 2005; Tracqui et al. 2008; Kamgoué et al. 2009). In the present study, full-field and long axis capture of beating myocytes with confocal microscopy provided overlapping sets of data to evaluate the specific effect of microrods on peak contraction.

Results here show that microrods promote greater magnitudes of auxotonic shortening or displacement in cardiac myocytes. Over 5 days, the local presence of microrods in 3D also affects certain anisotropic characteristics of myocytes. Furthermore, there was evidence that contractile changes due to microrods are dependent on certain aspects of RhoA/ROCK and PKC signaling, pathways previously implicated in hypertrophic and mechanosensing responses in cardiac myocytes. This study thus describes a novel way of both introducing and monitoring a set of physical cues that are important to the form and function of cardiac cells.

2 Materials and methods

2.1 Microrod fabrication

The fabrication of microrods by photolithographic techniques has been previously described in detail (Norman et al. 2008; Ayala et al. 2010). Briefly, negative photoresist SU-8 2010 (Microchem, Newton, MA) was spun onto the cleaned and dehydrated surface of a 3-in. silicon wafer. When a uniform thickness of 15 μm was reached, the wafer and photoresist were pre-baked and subsequently exposed to a 365 nm light source (13 mW/cm^2 for 13 s) through a custom transparency mask (Infinite Graphics, Minneapolis, MN). The wafer was then post-baked, and uncrosslinked SU-8 was removed with a developer solution (Microchem). The remaining fully formed 100 × 15 × 15 μm (L × W × H) microrods were collected from the wafer surface with 70% ethanol, washed in sterile phosphate-buffered saline (PBS), and stored in serum-free cell culture media.

2.2 Suspending cardiac myocytes and microrods in 3D

Primary ventricular myocytes were isolated from neonatal Sprague-Dawley rat hearts using an established enzymatic method (Motlagh et al. 2003a), as approved by UIC according to Institutional Animal Care and Use Committee and National Institutes of Health (NIH) *Guide for the Care and Use of Laboratory Animals* (NIH Publication 85-23, Rev. 1985). Myocytes and microrods were suspended in a 3D gel matrix using a variation in a previously published protocol (Curtis et al. 2010). The gel matrix used was the commercially available Matrigel extract (BD Biosciences, San Jose, CA), an extracellular matrix protein mixture purified from mouse sarcomas. For certain experiments, Matrigel was supplemented with submicron polystyrene beads (2.91×10^9/mL), each with a diameter of 0.5 μm (Molecular Probes, Eugene, OR), to assist in the tracking of cell contraction. When liquefied Matrigel was seeded with microrods and cells and allowed to polymerize on 35- mm glass-bottom dishes (MatTek, Ashland, MA), gel layers (0.5–1.0 mm in depth) containing the randomly distributed constituents were formed (Fig. 1a, b). The concentrations of myocytes (4×10^6/mL) and microrods (4×10^4/mL or 0.09% total volume) resulted in cells that were positioned no greater than 150 μm from a microrod (Curtis et al. 2010). As a whole, the bulk gel layer had stiffness values of shear modulus G' (22.9 Pa) and loss modulus G" (1.3 Pa) that were not affected by inclusion of the rigid microrods (Norman et al. 2008). Cell-seeded gels were provided fresh complete medium daily containing DMEM F-12 without L-glutamine (Sigma, St. Louis, MO), 5% fetal bovine serum, 1 mg/mL penicillin G/streptomycin, and 8 μM cytosine β-D-arabino-furanoside (Sigma, St. Louis, MO). In all experiments, cells were maintained at 37°C with 5% CO_2 for a total 5 days.

2.3 Live image capture of cardiac myocyte contraction

After 5 days of culture, cardiac myocytes were incubated with 5 μM Calcein AM (Invitrogen, Carlsbad, CA), a green fluorescent vital dye that allowed for beating cells to be more easily located in 3D gels. Myocyte contraction within the gel was recorded at the thickest region of each cell using a Zeiss LSM 510 META laser confocal microscope (Zeiss, Peabody, MA). To keep the compensations of 2D imaging to a minimum, only contracting myocytes that exhibited a long axis orientation flush with the optical stage (or xy-plane) were captured. Each image was collected as an optical slice from a differential interference contrast grayscale channel using a 63*x* magnification, 1.2 numerical aperture, water-immersion objective. Sequential 512 × 512 pixel images were taken approximately every 700 ms over a total of 1 min. From this time series, a pair of images representing states of rest (diastole) and peak contraction (systole) was selected for later analysis. A subsequent line scan sampling across each cell, capable of over 160 sweeps per second, was used to verify that the approximate endpoint of contraction was suitably captured.

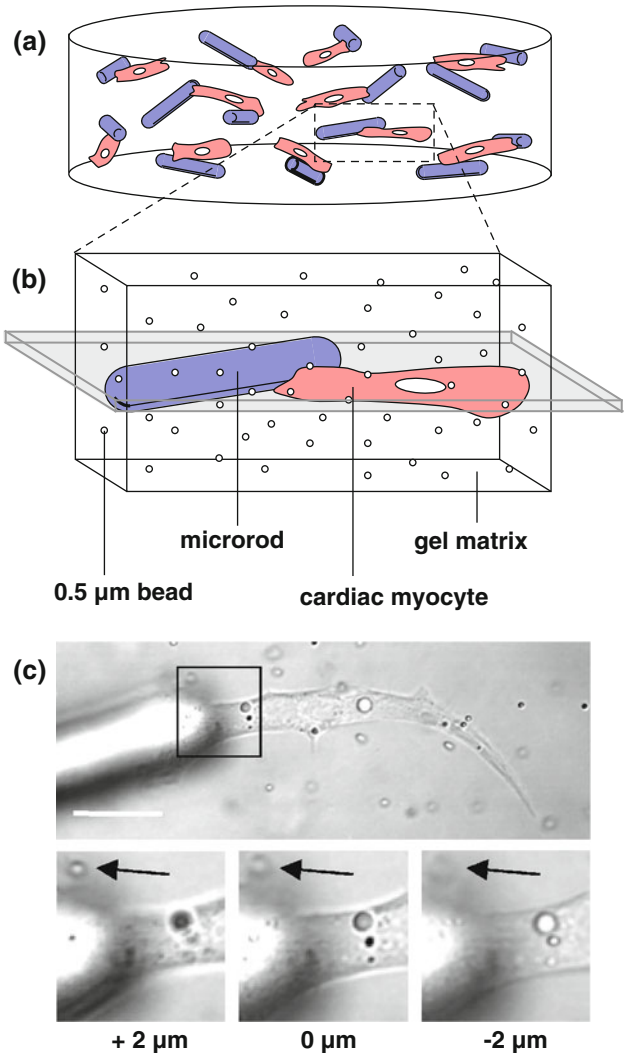

Fig. 1 Live imaging of 3D-suspended cardiac myocytes. **a** Isolated ventricular myocytes (*red*) are seeded in 3D gel matrices with 100 × 15 × 15 − μm rod-shaped polymeric microrods (*blue*). Cells and microrods are supported in the 0.5–1.0- mm thick gel layers with random orientation. **b** Individual myocytes with or without microrod abutment are imaged to track live contraction based on displacement in the visible plane (*shaded gray*). The presence of submicron beads, also added during initial seeding, serves to visualize movement in the nearly transparent gel. **c** Confocal microscopy is used to image live myocytes within a plane parallel to the optical stage (scale = 20 μm). *Black arrows* on *inset* zooms mark an in-plane tracking bead at the given focus depths. In experiments, this plane of detectable motion is between 4–8 μm, which coincides with the approximate thickness of most myocytes

2.4 Digital image correlation and full-field kinematic reconstruction

Images of myocytes at rest and peak contraction were processed for in-plane deformation measurements using a technique known as digital image correlation (Sutton et al. 1986; Doumalin et al. 1999, 2003; Budyn and Hoc 2010). Briefly, pixel tracking was performed by cross-correlation between successive grayscale images, where homogeneous deformations were assumed in separate cell, gel, or microrod phases. A zero-centered, normalized formulation for this cross-correlation was chosen, given that such a formulation is independent of the luminosity or light contrast that may vary between images (Doumalin 2000; Zhang et al. 2003). Pixels were tracked at regularly spaced points on a grid (typically 20 × 20) defined over the resting cell reference image. Changes in pixel positions (from rest to the deformed, contracting state) were identified by grayscale gradients in the vicinity of each grid point, and the recognition of pixel location corresponded to a calculated minimum correlation coefficient. In instances when pixel location was not detected, points were corrected using manual linear interpolation of 3 adjacent points that were accurately identified.

To reconstruct the continuous displacement field from the readings obtained by image correlation, a triangular mesh was generated over a sample image using the program Gmsh (Geuzaine and Remacle 2009). The mesh was made to conform to the explicitly defined cell and microrod boundaries contained in each image, as digitally surveyed with the program Plot Digitizer (Smith 2007). The point locations where displacements had been detected were then reinserted into the mesh by local adaptivity and used as the Dirichlet boundary condition of a finite element model. Finally, the scaled data were visualized as a continuous displacement field in and around single myocytes. From the resulting kinematic information, the cell area and perimeter could be exported, as well as values of the maximum displacement experienced within the cell and the average displacement occurring across the apparent cell area. The overall robustness of the displacement detection in images was consistent and, with the help of the dispersed submicron beads, free of sizeable errors. Correlation of two separate control images of a myocyte at rest yielded negligible displacement values, far less than those identified between images at rest and peak contraction.

To calculate the normal and shear strain fields from each displacement field, the different material phases in images were modeled as a linear elastic continuum. The resulting strain was then used to evaluate the maximum principal strain (magnitude and direction) present within each element face. The contributions of maximum principal strain to all elements within the cell were classified into two groups, with angles sorted into those from 0 to 20° (considered aligned) and those from 20 to 90° (considered unaligned) relative to the myocyte long axis. The element area occupied by this aligned and unaligned maximum principal strain, irrespective of magnitude, was tallied for the given cell sample. The total contribution of these element areas in each cell (or principal strain proportion) was also plotted in terms of the same 20° alignment cutoff. A total of 10 image pairs were analyzed for myocytes with or without microrods present.

2.5 Capture and analysis of axially positioned line scans

Similar to whole field capture of live cells, spontaneously beating myocytes displaying an axis of shortening parallel to the xy-plane were centered in focus under a laser confocal microscope with a 63× objective (Zeiss). Through the microscope software, a scanning line was positioned along the long axis of each myocyte, which often corresponded with the direction of greatest shortening. A single line was 1,024 pixels wide, bearing a pixel resolution between 0.03 and 0.08 μm/pixel depending on the length of the cell. Transmitted light from a differential interference contrast channel was captured from each line every 6.14 ms over the course of 30 s, thereby recording multiple complete and regular cycles of cell contraction. The semi-transparency of myocytes and the surrounding gel provided various grayscale features of intracellular particles, membrane folds, external tracking beads, or microrods that could be observed to displace during contraction. The result was an image of contractile motion over time, similar to a kymograph time-space-plot where the intensity along a line (x-axis) is stacked in sequence over time (y-axis). From the cell-generated motion, peaks of contraction could be easily discerned and used to mark states of maximum shortening. Image processing software (ImageJ, NIH, Bethesda, MA) allowed for these peaks to be scaled and measured along each axis to obtain the shortening time (in ms) and the maximum displacement (in μm) of a single cell. The identification of such peaks involved manual measurements but was fundamentally similar to fast Fourier transforms that have been automated for frequency analysis of any axial cell displacement (Goldyn et al. 2009). Additional quantification of displacements at 5 μm spaced positions along each line scan permitted calculations of the average displacement and the span of the greatest (upper 50%) displacements exhibited along the total cell length. A total of 8–14 line scans were captured, quantified, and averaged for cells in each experimental group and were representative of at least 3 separate cultures.

2.6 Fluorescent staining and imaging of cardiac myocytes

Cells in 3D gels were fixed in 2.0% paraformaldehyde for 10 mins, followed by a 0.3 M glycine/PBS rinse. Seeded gels were then incubated in 0.5% Triton X-100 (Sigma) for 10 min to permeabilize cell membranes, followed by 10%

goat serum/PBS for 20 min to block nonspecific binding activity. Cells were labeled for 1 h with an antibody for sarcomeric α-actinin (mouse monoclonal ab9465, Abcam, Cambridge, MA) diluted 1/200 in 1% bovine serum albumin (BSA)/PBS. After 3 PBS washes, cells were incubated with goat anti-mouse Alexa Fluor IgG 568 secondary antibody (Invitrogen) diluted 1/1,000 for 45 min. Alternatively, myocytes requiring no immunolabeling were stained with rhodamine phalloidin (Invitrogen) diluted 1/200 in BSA/PBS for 1 h. All gels were then rinsed with PBS and stored in 1 nM 4',6-diamidino-2-phenylindole (DAPI)/PBS (Vector Labs, Burlingame, CA) until imaged. Fluorescence was captured as single 1 μm optical slices and 1024 $\times$ 1024 pixel images using a laser confocal microscope with a 63x or 25x objective, a setup similar to that described earlier.

2.7 Image analysis of stained cardiac myocytes

Measurement of myocyte size in fluorescent images was based on α-actinin signals indicative of total sarcomeric content in muscle cells. Within each image, a stereological average of individual striated cell areas was determined using ImageJ software. Scaled areas (in μm^2) were then normalized to the negative control group (containing no microrods or treatment) from each culture. A total of 18 images were taken for each experimental condition over 3 independent cultures.

Assessment of myofibril alignment in myocytes was also performed with ImageJ but was based on phalloidin staining of filamentous actin in higher magnification images (Bray et al. 2008). A previously published method of systematic binning was used with the software to compartmentalize all visible myofibrils within a cell (Karlon et al. 1999; Kaunas et al. 2005). Briefly, the phalloidin signal was first converted to a grayscale, and the average pixel intensity in a full cell of interest was recorded. Next, a scaled grid with a subregion size of 2.5 μm (6.25 μm^2) was superimposed on the cell. For each grid square, the average pixel intensity was again measured; subregions with intensities less than 40% of the total cell average were discarded. If the signal in a subregion was strong enough, a line was overlaid along a row of sarcomeres. The angle of this line was recorded, and the process was repeated for every subregion contained within the cell. Angles were normalized from 0° to 90° relative to the determined long axis of each myocyte, which was typically assigned along the axis of greatest myofibril alignment. The total subregion area per angle was counted for each cell, with angles categorized into groups less than or greater than 20°. This same angle cutoff has been used previously to define aligned and unaligned myofibrils in cardiac myocytes (Chopra et al. 2011; Parrag et al. 2011). The cellular proportion of areas for the aligned or unaligned groups was also plotted. All quantifications were averaged from 15 images of each blinded condition acquired over 3 cultures. A sampling of the analysis was repeated by an additional unbiased observer, which yielded consistent differences between experiment groups.

2.8 Inhibition of RhoA/ROCK, FAK, and PKC signaling

To identify key molecular signals involved in the cellular recognition of microrods, several pathways were disrupted via long-term pharmacological inhibition. These agents included cell permeable C3 Transferase (Cytoskeleton, Denver, CO), which inactivates Rho GTPases via ADP-ribosylation, the compound Y-27632 (Sigma), which blocks the catalytic site of ROCK, and the MLCK inhibitor ML-7 (Sigma) (Isemura et al. 1991; Uehata et al. 1997). Also used was the chemical GF109203X (Tocris, Elliswille, MO), which outcompetes ATP on several PKC isoforms, and PF-573228 (Tocris), which potently inhibits tyrosine phosphorylation of FAK (Toullec et al. 1991; Slack-Davis et al. 2007). Stock solutions of C3 Transferase, Y-27632, ML-7, GF109203X, and PF-573228 were prepared and stored in sterile H_2O or dimethyl sulfoxide (DMSO) according to the recommendations of each manufacturer. Working solutions of inhibitors were made fresh with warm culture media and added to 3D cultures for storage at 37°C. For these solutions, less than 0.1% DMSO by volume was added to media, a threshold that has been reported to have no effect on intracellular calcium concentrations (Zhou et al. 2002). Cells were treated with Y-27632 (10 μM) and PF-573228 (1 μM) over 72 h, C3 Transferase (0.3 μg/mL) for 36 h, and ML-7 (20 μM) and GF109203X (10 μM) for 24 h, with supplemented media changed daily as needed.

2.9 Evaluation of protein content in cardiac myocytes

An assessment of myocyte size was carried out for 3D-cultured cells by determining the ratios of total protein levels to cell numbers. Briefly, viable cells were removed from gels by incubation with 400 μL Dispase (BD Biosciences) for 2 h at 37°C. Cells were collected, pelleted, resuspended in PBS, and split into two volumes—one of which counted (n = 5) using trypan blue (Cambrex, East Rutherford, NJ) and a hemocytometer. The remaining cells were lysed with 100 μL 1% SDS buffer, and protein levels were measured with a Qubit fluorometer and Quant-iT protein assay (Invitrogen). Ratios of protein readings to respective cell counts were averaged from each group and normalized to those from 3D gels with no microrods or treatment. The average fold changes from 3 separate cultures were then reported.

2.10 Western blotting for analysis of FAK expression

Myocytes were cultured on 2D surface-modified polystyrene dishes (Becton Dickinson, Franklin Lakes, NJ), with or without exposure to 1 μM PF-573228 in media changed daily over 72 h. Cells were scraped over ice in 1% SDS buffer containing protease and phosphatase inhibitor cocktails (Sigma). Collected lysates were then briefly sonicated and pelleted by centrifugation at 14,000×g for 15 min. The protein content in the supernatant was then measured and equilibrated, and corresponding volumes were diluted 1:1 with Laemelli sample buffer (Bio-Rad, Hercules, CA) containing 5% 2-mercaptoethanol (Sigma) and boiled at 100°C for 5 min. Approximately 25–40 μg of protein was loaded onto and resolved within a Criterion Tris–HCl 10% polyacrylamide gel (Bio-Rad), followed by transfer to a methanol-activated polyvinylidene fluoride (PVDF) membrane (0.2 μm, Bio-Rad). After blocking with 5% nonfat milk in Tris-buffered saline—0.05% Tween 20 (TBST), membranes were probed with antibodies for total FAK (rabbit monoclonal ab40794, Abcam), tyrosine 397-phosphorylated FAK (rabbit polyclonal ab39967, Abcam), and glyceraldehyde-3-phosphate dehydrogenase (GAPDH, rabbit polyclonal ab9485, Abcam) diluted in 1% BSA-TBST. Unbound antibodies were removed with copious rinsing with TBST, and membranes were then incubated with an anti-rabbit IgG horseradish peroxidase (HRP)-linked antibody (Cell Signaling, Beverly, MA) in 1% BSA-TBST. After additional TBST washes, bands were visualized by enhanced chemiluminescence (ECL, GE Healthcare, Piscataway, NJ) and captured with a ChemiDoc XRS+ molecular imager and ImageLab software (Bio-Rad).

2.11 Statistics

Statistical analysis was performed using Excel software (Microsoft, Redmond, CA) and specialized JavaScript functions (VassarStats, Poughkeepsie, NY). Differences in quantitative variables were calculated by a two-tailed Student's t test or one-way ANOVA for independent samples. The Tukey–Kramer *post hoc* test was used to determine significance for multiple conditions. All data are expressed as mean ± SEM, with significance marked as $p < 0.05$.

3 Results

3.1 Aspects of cardiac myocyte displacement

For this study, the analysis of motion in 3D-suspended cardiac myocytes was restricted to those cells within a defined image plane. With the given confocal microscopy setup, this image plane corresponded to a theoretical depth of focus (or z-axis depth) of nearly 1 μm. However, height-dependent recording of the cell-seeded gels showed that individual submicron tracking beads typically came in and out of focus at a span of 4–8 μm (Fig. 1c). This range was similar to the approximate thickness of myocytes in 3D, thus establishing a consistent plane in which to track whole cells and their perturbed surroundings.

Under controlled seeding densities of cells and microrods, most spontaneously contracting myocytes found within the xy-plane showed single end attachment with 1 microrod (as depicted in Fig. 1). In rare instances, a flanked configuration of a myocyte contracting between 2 microrods was observed in the same plane. In both situations, the 100 − μm-long microrods could often be seen to move within the soft supporting gel matrix during cyclical beating of the adjacent myocyte. That is, a discrete microrod was pulled elastically toward the cell as it contracted, returning to its original position in the gel as the myocyte relaxed (see Online Resources 1-3).

After 5 days of 3D culture, myocytes residing near a microrod adopted different mechanical characteristics than cells in control gels with no added microrods. Such changes were most apparent in terms of the displacement exhibited by myocytes during peak contraction. Correlation of images taken at rest and peak contraction allowed for these in-plane displacement values to be precisely quantified over single cell fields (Fig. 2a, d). As a whole, myocytes generated greater magnitudes of displacement in the presence of microrods (note the scales of Fig. 2b, d). Similarly, values of the maximum displacement detected, as averaged across multiple cells, were found to be significantly higher in microrod-attached myocytes (1.91 ± 0.49 μm) than myocytes in gel alone (0.65 ± 0.15 μm) (Fig. 2e).

3.2 Axial mechanics of cardiac myocytes

In a separate, more simplified method of mechanical analysis, single-pixel-wide line scans were used to capture the longitudinal (or axial) displacement of beating myocytes. These scans were intended as a means to not only validate the microrod-related changes in cell displacement, but also to repeat the measurements with respect to the time of the contraction cycle. Myocytes in conditions with or without microrods both displayed a predominantly bipolar shape, and cells within the xy-plane thus had an easily identifiable long axis for the placement of a scanning line. Each scaled line scan permitted quantification of shortening time and displacement at regular intervals (5 μm) along the given axis (Fig. 3a, b). From recorded displacement values, the maximum displacement was determined for each cell, an index similar to those reported from the full-field analysis. In addition, the axial span of the greatest displacement values (>50% of

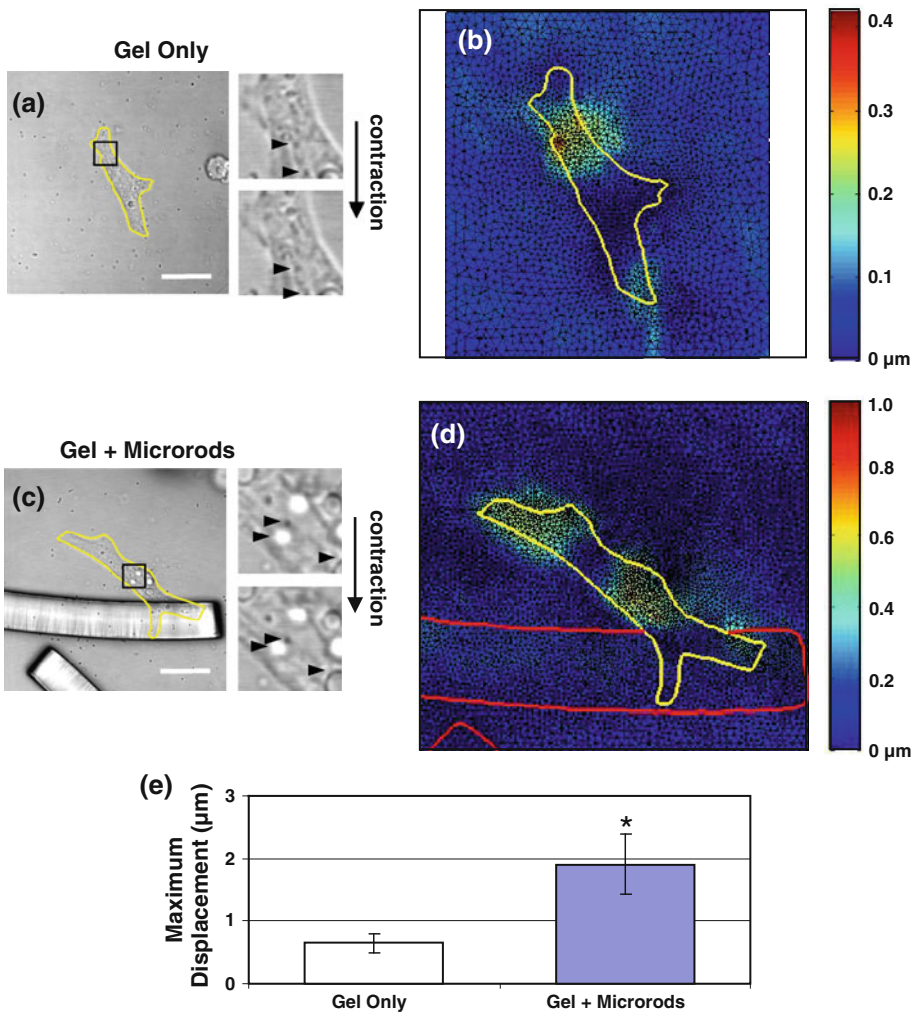

Fig. 2 Cardiac myocyte displacement is affected by 3D-suspended microrods. **a, c** Grayscale images of xy-plane oriented myocytes (*yellow outline*) at states of rest (diastole) and peak contraction (systole) were exported from a confocal microscopy time series (*scale* 20 µm). *Inset* zooms of these two states illustrate the snapshot change in motion of all trackable particles and features; some sample positions are marked with *black arrowheads*. **b, d** Correlation of images reveals the range of displacements in active myocytes, falling between 0.2–0.4 µm in the example shown. With microrod abutment, myocyte displacement is greater in magnitude, reaching 1.0 µm in the given example (note the differences in scales between the two colormaps). **e** Quantification of such observations across pooled samples ($n = 5$ per condition) shows that myocytes with adjacent microrods display significantly higher maximum displacement values (1.91 ± 0.49 µm) than control cells (0.65 ± 0.15 µm). Mean ± SEM. * $p < 0.05$

maximum) was noted as a way to assess the overall non-uniformity of myocyte shortening.

When associated with a microrod, myocytes produced significantly higher values of maximum displacement axially (3.08 ± 0.34 µm) compared to control cells (1.79 ± 0.12 µm) (Fig. 3c). These shifts mirrored results from the image analysis detailed earlier (see Online Resource 4 for comparison of sample data from both methods). Though the total length of the long axis was greater for myocytes growing with microrods (57.48 ± 2.98 µm) than myocytes in uniform gels (47.63 ± 2.69 µm), the span of the greatest displacement along this axis was significantly smaller when microrods were present (21.73 ± 2.16 µm versus 27.98 ± 2.08 µm) (Fig. 3d). For cells with microrods, the greatest displacement values occurred at an average position of 29.7 ± 4.4 µm distal from the microrod, which corresponded to an axial location near the center of myocytes (not shown). Beyond this, the high time resolution of line scans showed that myocytes with microrods experienced significant decreases in shortening time (from 217.4 ± 10.1 ms to 171.2 ± 9.1 ms) (Fig. 3e). Altogether, a simple ratio of maximum displacement to shortening time indicated that the shortening velocity of myocytes increased over twofold with microrod inclusion (Fig. 3f). Results were supported by earlier data concerning increased SERCA2 levels and the potential for modified excitation–contraction coupling with microrods (Curtis et al. 2010).

3.3 Myofibril alignment and maximum principal strain

One contributing factor to altered mechanics in force-generating cells is intracellular architecture. To examine the effect of microrods on actin organization, 3D-seeded myocytes were fixed and stained with phalloidin (Fig. 4a, b). Orientations of myofibrils, the actomyosin contractile machinery in muscle cells, were surveyed by angle of deviation ($0-90°$) relative to the myocyte long axis. The area of myofibrils aligned with the long axis ($\leq 20°$ deviation) was significantly greater in myocytes with microrods (483.3 ± 50.8 µm^2) than in control myocytes (253.3 ± 18.9 µm^2), yet no difference

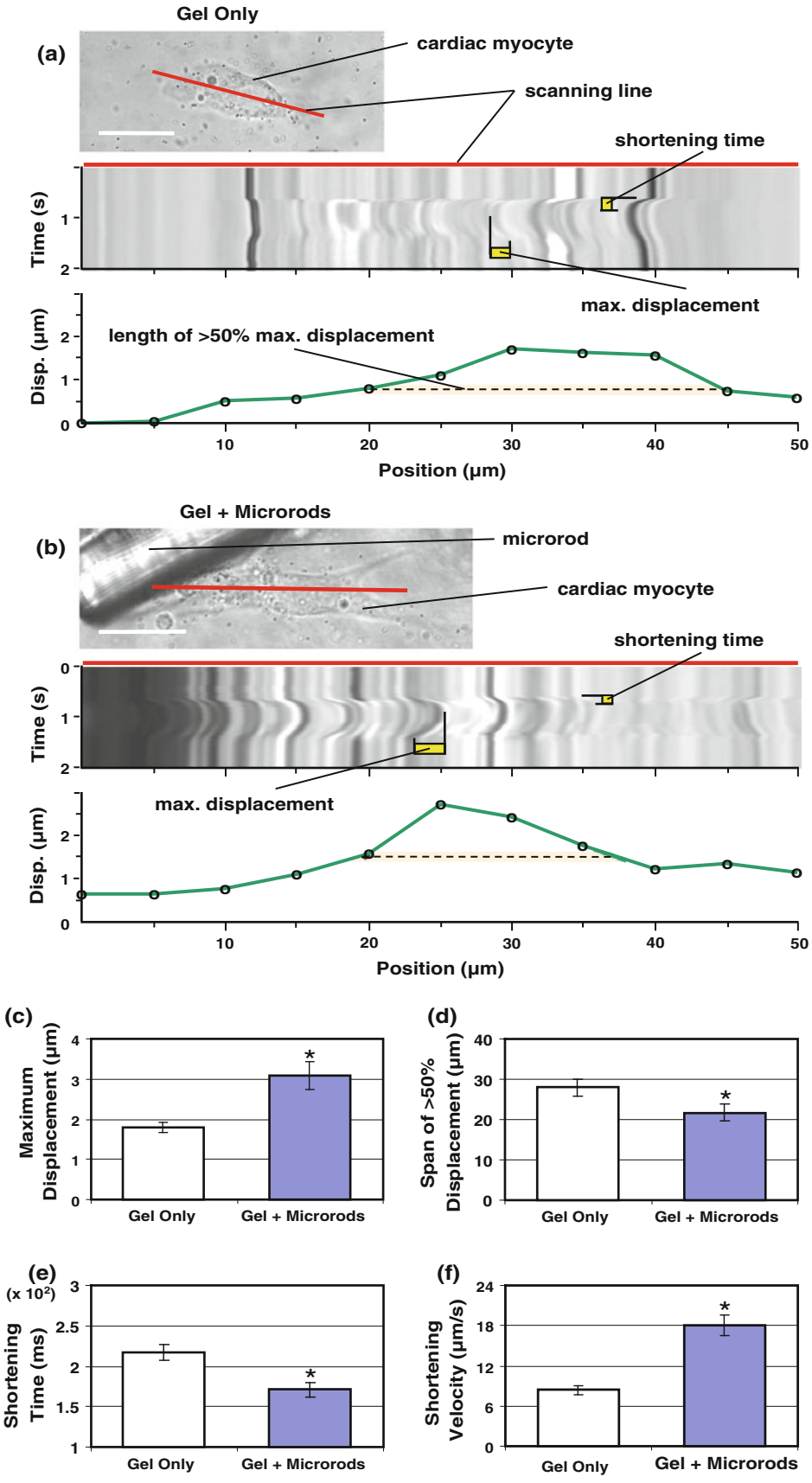

Fig. 3 Axial mechanics of cardiac myocyte contraction are influenced by microrod presence. **a, b** Rapid traces along the long axis of single myocytes with or without local microrods (*scale* 20 µm) were captured as a one-dimensional time series (or a *line scan*, with placement designated by *red line*). From each scaled line scan, offline measurements of shortening time and maximum displacement could be made for individual myocyte beats. Cell displacement was also measured at 5 − µm intervals (*green line* in plot) along the span of each line scan, which was used to determine the axial span (*dashed orange line*) of the greatest displacements (>50% of maximum). **c** Myocytes abutting a microrod exhibit significantly higher maximum displacements (3.08 ± 0.34 µm) than cells in gels with no microrods (1.79 ± 0.12 µm) ($n = 26$ scans total). **d** The axial span of the greatest displacements is smaller in myocytes with adjacent microrods (21.73 ± 2.16 µm) than in control cells (27.98 ± 2.08 µm). **e** Microrod inclusion causes a decrease in the shortening time of myocytes (from 217.4 ± 10.1 to 171.2 ± 9.1 ms). **f** A simple index of shortening velocity (maximum displacement/shortening time) is found to be significantly higher in microrod groups (18.02 ± 1.59 µm/s) compared to control cells (8.42 ± 0.70 µm/s). Mean ± SEM. * $p < 0.05$

was found between areas of unaligned myofibrils (>20° deviation) (Fig. 4c). These results, when expressed as fractions of total cell areas, revealed that the addition of microrods caused significant increases in the overall proportion of aligned myofibril area (from 0.63 ± 0.03 to 0.77 ± 0.03) (Fig. 4d).

To determine whether the microrod-affected alignment of myofibrils could be directly compared with a change in contractile mechanics, maps of principal strains from live myocytes were evaluated. Displacement data collected from the full-field analysis were used to calculate the directions of maximum principal strain occurring in myocytes at peak contraction (Fig. 4g, j). The angles (0–90°) of these principal strain directions were again grouped by relative alignment with the assigned long axis, marked by deviations of 20° or less. However, no statistical significance could be found for pooled data in the available sample size. Specifically, increases in average area of axially aligned maximum principal strain were not statistically different for conditions with microrods ($416.6 \pm 185.3\,\mu m^2$) over controls ($254.6 \pm 51.8\,\mu m^2$) (Fig. 4k). The maximum principal strain aligned with the long axis also existed in slightly greater cellular proportions when microrods were present (0.56 ± 0.02 compared to 0.43 ± 0.06), but the p value of this sampling failed the significance level of 0.05 (Fig. 4l).

3.4 Dependence of axial mechanics on RhoA/ROCK and PKC signaling

It was hypothesized that the ability of microrods to influence myocyte behavior was dependent on several well-known intracellular signals involved in mechanosensing and actin-regulating processes. To help address this, line scans of axial displacement provided a straightforward way to quantify the mechanical result of interrupting such signals over the long-term ($\geq$24 h) in myocytes. Accordingly, readouts of maximum displacement (Fig. 5a) and shortening velocity (Fig. 5b), which were significantly different in microrod and control groups, showed no response to microrods upon the inhibition of the RhoA/ROCK pathway. Specifically, myocytes exposed to Rho inhibitor C3 Transferase (0.3 μg/mL for 36 h), ROCK inhibitor Y-27632 (10 μM for 72 h), or myosin light chain kinase inhibitor ML-7 (20 μM for 24 h) displayed no significant changes in maximum displacement or shortening velocity regardless of microrod inclusion. Inhibition of PKC isoforms with GF109203X (10 μM for 24 h) also ablated the differences in maximum displacement and shortening velocity due to microrods. In contrast, the effects of microrods were upheld after inhibition of an activated form of FAK with the potent compound PF-573228 (1 μM for 72 h), though values of maximum displacement were diminished overall with the treatment. These outcomes suggest that the activity of PKC and certain RhoA/ROCK pathway constituents play key roles in eliciting microrod-related mechanical changes in cardiac myocytes.

3.5 Microrod-induced cell growth and RhoA/ROCK inhibition

It was previously reported that microrods in 3D gels can stimulate increases in myocyte size and protein content indicative of hypertrophy (Curtis et al. 2010). However, it was unclear whether the RhoA/ROCK pathway also participated in this growth response. Cells were thus analyzed after 5 days in 3D culture with or without microrods and compared to similar groups treated for 72 h with 10 μM Y-27632 (Fig. 6a–d). Quantification of cell area (via muscle-specific α-actinin staining) showed that the significant fold increase in myocyte size caused by microrod addition (1.34 ± 0.07) was prevented with long-term inhibition of ROCK (Fig. 6e). In addition, measurements of protein levels per total cell populations, ratios which were significantly increased by microrods (1.27 ± 0.03), demonstrated no such differences upon Y-27632 treatment (Fig. 6f). Both results coincided with the RhoA/ROCK involvement in microrod-altered cell mechanics described earlier.

4 Discussion

Results show that the interaction of individual myocytes with regions of heterogeneity influences the mechanics of contraction. Over time, these contiguous polymeric microrods induce differences in cell displacement and the extent of axially aligned myofibrils. Several of these long-term changes were affected by the inhibition of RhoA/ROCK and PKC signaling. Microdomain heterogeneity, as detected by single cells in 3D, can thus play a major role in the mechanobiological regulation of cardiac myocytes.

4.1 Altered kinematics of microrod-interacting cardiac myocytes

When the in-plane contractile motion of myocytes was measured using separate full-field and axial-based imaging methods, values of maximum displacement were found to be consistently increased with microrod contact. Yet interestingly, these greater cell displacements were contained over a smaller axial distance when microrods were present, an apparent localization of the most active contractile motion (Fig. 3d). This phenomenon could indicate that microrods cause a redistribution of intracellular tension in myocytes. The inclusion of relatively large, cell-scaled, rigid microrods would be likely to serve as loads to single myocytes, and thereby increase the local stiffness in 3D. However, these loads were not held fixed, as microrod-associated

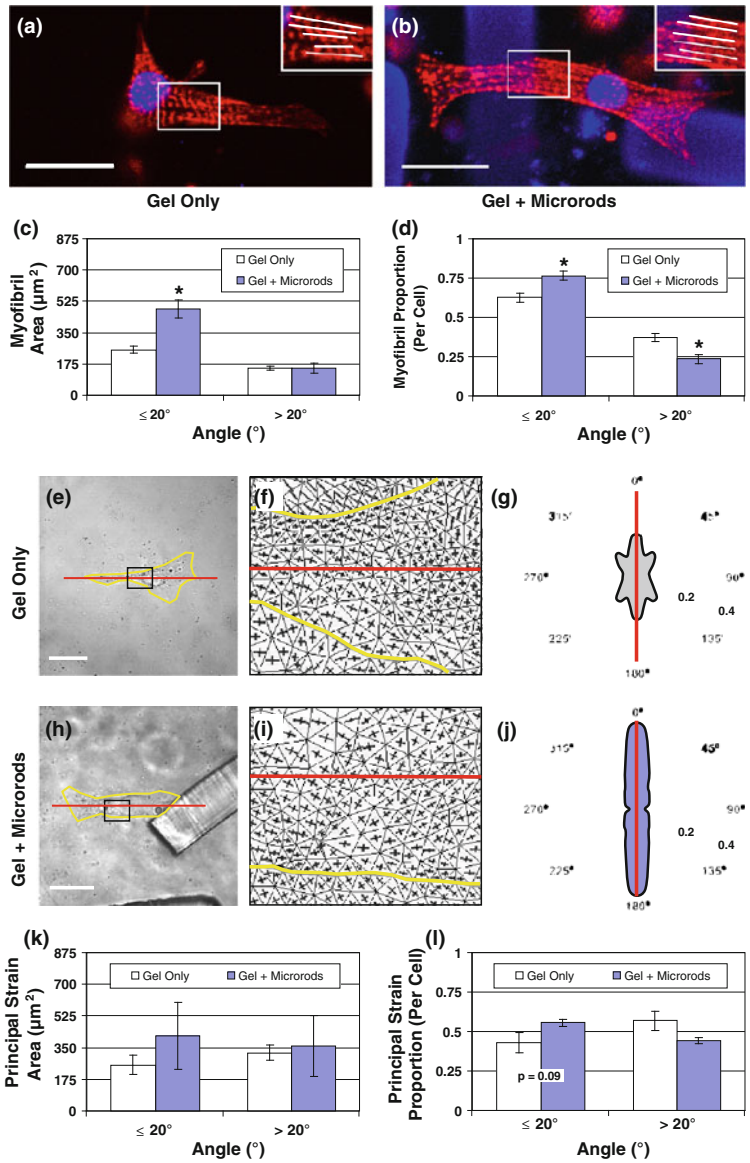

Fig. 4 Effect of microrods on myofibril orientation and axial alignment of principal strain in cardiac myocytes. **a, b** Myocytes with or without microrods in 3D gels were fixed and stained for actin (rhodamine phalloidin, *red*) and nuclei (DAPI, *blue*). Note that microrods also appear blue (*scale* 20 μm). Myofibrils and their predominantly longitudinal orientation can be distinguished in the *inset* zooms. **c** Images from fluorescent staining were analyzed to survey the orientation of myofibrils within regular 2.5 − μm *square regions*. The total area of myofibril angles equal or less than 20° (deviation relative to myocyte long axis) is significantly higher in cells with microrods (483.3 ± 50.8 μm^2) than in control cells (253.3 ± 18.9 μm^2), but no difference exists between the area of unaligned myofibrils greater than 20° (n = 15 cells per group). **d** The proportion of aligned (≤ 20°) myofibril area in cells is significantly higher in the presence of microrods (0.77 ± 0.03) compared to cells with no microrods (0.63 ± 0.03); the reverse is true for the proportion of unaligned (> 20°) myofibril area. **e, h** Images of single myocytes (*yellow outline*) in gel alone or with microrods were correlated from states of rest and peak contraction (*scale* = 20 μm). **f, i** Strain data were collected for images sets of each condition and used to calculate the maximum and minimum principal strain vectors (represented as orthogonal lines) that occur at points within the captured field. The areas shown are zooms of the insets shown in **e** and **h**. The long axis of each cell is also marked (*red line*). **g, j** The fraction (normalized by cell area) of maximum principal strains by angle (relative to the assigned long axis, *red line*) is displayed within polar plots of each example. **k** All principal strain data averaged across multiple cells (n = 5) yield no statistical significance, but did show trends that supported the more extensive myofibril analysis. Accordingly, the average area of maximum principal strain is identified at angles near the myocyte long axis (≤ 20°) in conditions with or without microrods. **l** Directions of principal strain are aligned with the long axis in slightly greater cellular proportions when microrods are present (0.56 ± 0.02 vs. 0.43 ± 0.06), but these differences are not significant. Mean ± SEM. * $p < 0.05$

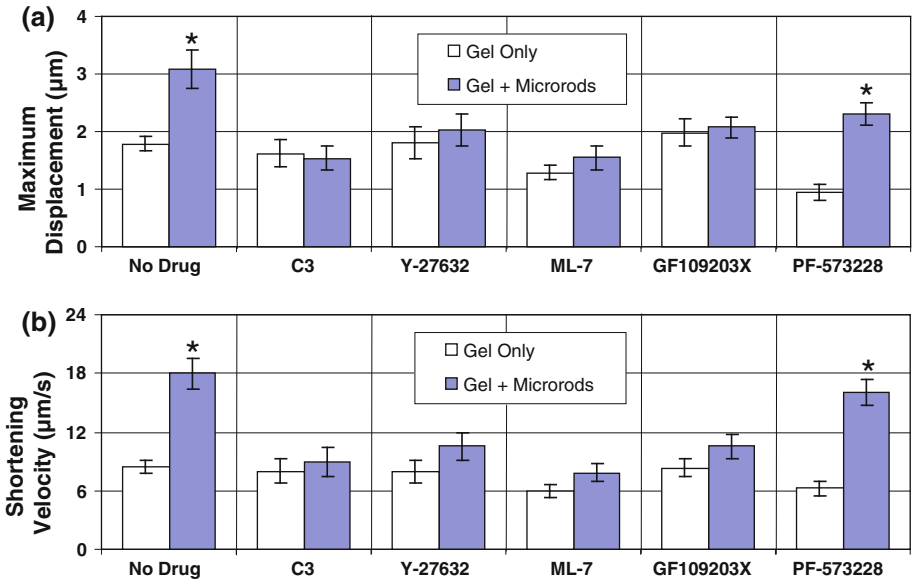

Fig. 5 Microrod presence affects the axial mechanics of cardiac myocytes via RhoA/ROCK signaling. Microrods cause significant changes in maximum displacement and shortening velocity for contracting myocytes (as assessed from line scans in Fig. 3). Differences in maximum displacement (**a**) and shortening velocity (**b**) are eliminated between microrod-containing and microrod-absent groups when effectors of the RhoA/ROCK pathway are targeted with ROCK inhibitor Y-27632 (10 μM for 72 h), Rho inhibitor C3 Transferase (0.3 μg/mL for 36 h), and myosin light chain kinase inhibitor ML-7 (20 μM for 24 h) (n = 18–20 scans for each drug). However, while inhibition of activated FAK with PF-573228 (1 μM for 72 h) caused slight decreases in maximum displacement and shortening velocity, it did not eliminate the significant effect of microrods. Mean ± SEM. * $p < 0.05$

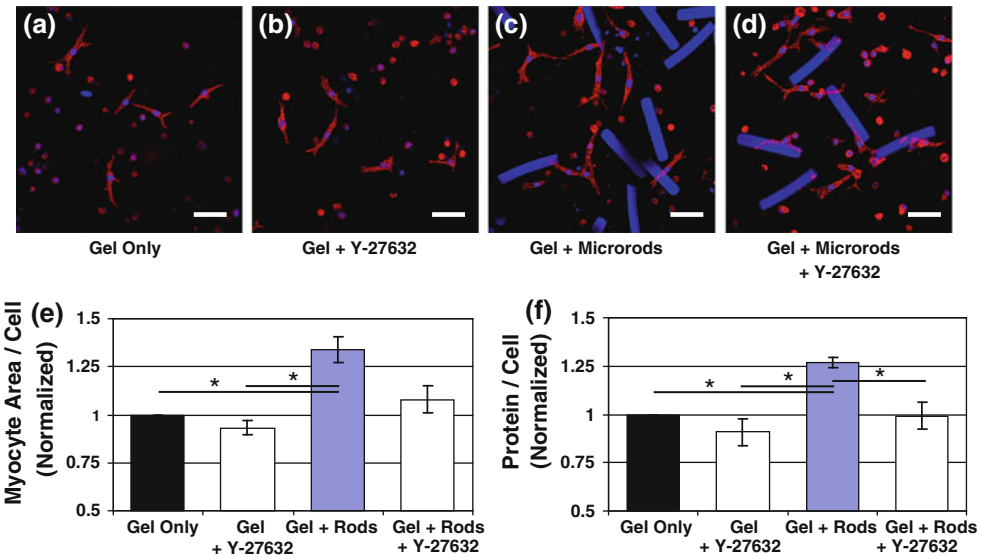

Fig. 6 Microrod-induced cardiac myocyte growth is dependent on the RhoA/ROCK pathway. Differences in cell size were assessed with laser confocal microscopy after 5 days in culture for myocytes in 3D gels (**a**), myocytes in gels treated for 72 h with 10 μM Y-27632 (**b**), myocytes in gels containing microrods (**c**), and Y-27632-treated gels with both myocytes and microrods (**d**). Cells were stained with antibodies for muscle-specific α-actinin (*red*) and nuclei (*blue*); microrods also fluoresce blue (*scale* 50 μm). **e** Analysis of cell area in images reveals that the significant increase in myocyte size caused by microrod addition ("*Gel + Rods*," 1.34 ± 0.07) is abrogated with long-term inhibition of ROCK (n = 3 cultures, 18 total images per condition). **f** Protein levels per total cell count in each gel show similar results, with no significant differences between gels with or without microrods upon Y-27632 treatment (n = 3). Mean ± SEM. * $p < 0.05$

myocytes could often be observed pushing the microrods through the soft and highly elastic supporting gel. Furthermore, the observed increases in maximum displacement could not be correlated with the actual 3D orientation between a given myocyte and microrod (not shown). With this model system, it is therefore the simple introduction

of 3D heterogeneity alone that affects the peak contractile behavior of cardiac myocytes.

Other studies of cardiac myocytes in 3D constructs have shown that contractile responses are largely dictated by the engineered surroundings. For example, embryonic ventricular myocytes seeded in tubular collagen scaffolds exhibit a steady transition from a quiescent to contractile phenotype (Evans et al. 2003). Similar contractile development of embryonic myocytes was also observed in more pliant, less densely populated collagen gels (Feng et al. 2003). Overall, myocytes in these 3D environments maintained spontaneous contractions 2–3 times longer (>45 days) than those on 2D cultures. Neonatal ventricular myocytes have been shown to exhibit regular contractions after being cultured between 3D gel layers of differing stiffnesses and filamentous protein concentrations (Bakunts et al. 2008). In addition, more highly organized patterns of myocyte displacement were found in relatively soft fibrinogen gels, bearing bulk shear moduli near those of gels used in current experiments (Shapira-Schweitzer and Seliktar 2007). Mechanical adaptation is known to be regulated by variation in the stiffness below the cardiac myocytes in a 2D substrate (Engler et al. 2008; Jacot et al. 2008). Since myocytes are of comparable size to the microrods, a similar phenomenon might be occurring here.

4.2 Microrods promote structural anisotropy in cardiac myocytes

It was previously reported that myocytes become hypertrophied after 10 days in 3D culture with microrods (Curtis et al. 2010), but comparative changes were also evident by day 5 in the current study (Fig. 6a, c, e, f). The microrod-attributed difference in striated area was found to be oriented with the long axis in myocytes (Fig. 4c), thereby affecting the proportion of aligned myofibrils of individual cells. This increase in alignment did not conflict with a more computationally intensive analysis of maximum principal strain in microrod-neighboring myocytes (Fig. 4k, l), though such a comparison could not be statistically confirmed. The result was thus myocytes demonstrating slightly more in vivo-like qualities of anisotropic behavior on account of microrod locality. This suggests that the amount of myofibrils in alignment, rather than the global order of the cell, drives the mechanical response to 3D heterogeneity. This can be supported by work with fibroblasts in 3D matrices, which has shown that a change in cell tension corresponds less with the overall alignment of contractile stress fibers than with the extent and number of those aligned fibers (Grinnell 2000).

Several other studies have reported an ability to control myocyte organization and anisotropy in vitro through various physical cues. On micropatterned 2D surfaces, the introduction of corners within adhesion-promoting areas (*i.e.* from circles to rectangles) was shown to induce local anisotropy of myofibrils in myocytes (Parker et al. 2008; Bray et al. 2008; Geisse et al. 2009). This myofibril anisotropy was seen to expand throughout the myocyte with certain defined geometric boundaries, which could consequently promote mechanical anisotropy during peak contraction (Bray et al. 2008; Grosberg et al. 2011). Above flat culture conditions, myocytes interacting with structures (5 μm high, 15 μm diameter) on elastomeric substrates were shown to terminate with sarcomeric striations over a greater thickness than cells on untextured substrates (Motlagh et al. 2003a,b). In a much larger scale, 1.5- mm-high elastomeric posts have been used to guide actin alignment across densely grown myocytes, resulting in an increase in anisotropic tension in cardiac muscle tissues (Bian et al. 2009). When seeded in 3D environments containing discontinuities of stiffness, fibroblasts are known to rebuild their cytoskeleton to polarize in the direction of the greatest effective stiffness (Bischofs and Schwarz 2003). Microrods thus appear to act as similar forms of local discontinuities, providing a combination of high stiffness and spatial heterogeneity in 3D to affect cardiac myocyte remodeling.

4.3 Mechanisms of microrod-affected cell responses

Prior work exploring the gene expression profiles of microrod-presented cells had identified no single, unifying mechanism of microrod action (Collins et al. 2010; Curtis et al. 2010). However, such RNA transcription data highlighted an overall importance of cell anchorage and actin cytoskeletal regulation in the responses to microrods. The relevance of these processes has been substantiated by recent research with fibroblasts, which proved that cell responses induced by either topographic or 3D heterogeneity were mediated by the RhoA/ROCK pathway (Patel et al. 2010; Ayala et al. 2010; Ayala and Desai 2011). For cardiac myocytes on 2D substrates, stretch-activated RhoA/ROCK signaling has shown a dependence on PKC function (Pan et al. 205). Yet, it remained to be seen whether the same effectors of actin dynamics were equally pertinent to 3D-suspended myocytes, given their less pronounced focal adhesions and spreading capability (Cukierman et al. 2001; Evans et al. 2003). The scope of the current study prevents a complete mechanism from being fully elucidated. However, the results of this study demonstrate that several targets related to the RhoA/ROCK pathway could, in fact, be specifically implicated in the long-term remodeling and mechanical changes caused by microrods.

The significant mechanical differences that existed between myocytes with or without microrod contact were abrogated with C3 Transferase, Y-27632, or ML-7 treatment; the overlap of these results underscores an involvement of RhoA/ROCK signaling. Similar findings with GF109203X (which targets PKC isoforms α, $\beta 1$, δ, ε, and ζ selectively)

suggest that the RhoA/ROCK dynamics occur downstream of PKC. Conversely, preservation of the mechanical differences between microrod and control groups with PF-573228 suggests that the kinase activity of FAK may be less important in microrod responses than its core scaffolding function. All such experimental comparisons were based only on measurements of axial displacement, which alone could not distinguish the effects of modified growth or anisotropy in cells. However, the RhoA/ROCK pathway was also confirmed to be required for microrod-induced hypertrophy, as the changes in cell size and protein content were prevented by 3 days of ROCK inhibition (Fig. 6e, f). This indicates that the RhoA/ROCK-dependent mechanics observed are a function of long-term cell remodeling and not contractility per se, though it is difficult to separate the two interrelated processes. Complicating this further, expression levels of the sarcoplasmic calcium pump SERCA2 have been reported to be significantly higher after 10 days with microrods (Curtis et al. 2010). While SERCA2 levels do not always correlate with increased calcium load and contractility, its expression can be a sign of broader maturation changes in response to physical cues (Moorman et al. 1995; Jacot et al. 2008). Even so, it has been shown that blockade of calcium transients alone does not prevent all aspects of a hypertrophic phenotype (such as cell size), and that mechanical activity itself is critical for remodeling changes (Eble et al. 1998). In all, it is clear that a certain pathway-specific mechanical feedback arises from stable microrod contact to alter myocyte contractile behavior (Fig. 7).

4.4 Limitations of the study

The main technical limitations of this work were related to the various compensations involved in live cell imaging. For one, the continuous beating of cells during whole image acquisition (via a nonresonant scanning system) was an issue that complicated the identification of peak contraction in myocytes. A comparison of displacement values from full-field and axial-based capture (Online Resource 4) confirms that the magnitude of maximum displacement was detected more accurately with the more rapid line scans; this was expected and remained the rationale for the overlapping methods. In addition, the correlation of images from myocyte rest and peak contraction meant that the analysis was based on merely a snapshot of mechanical changes, independent of shortening time. Finally, it must be restated that all assessments of images remained but a planar approximation of contractile events, albeit from cells afforded a full 3D environment.

4.5 Conclusions

In all, the findings demonstrate that microdomain heterogeneity in 3D alters the local mechanics exhibited during

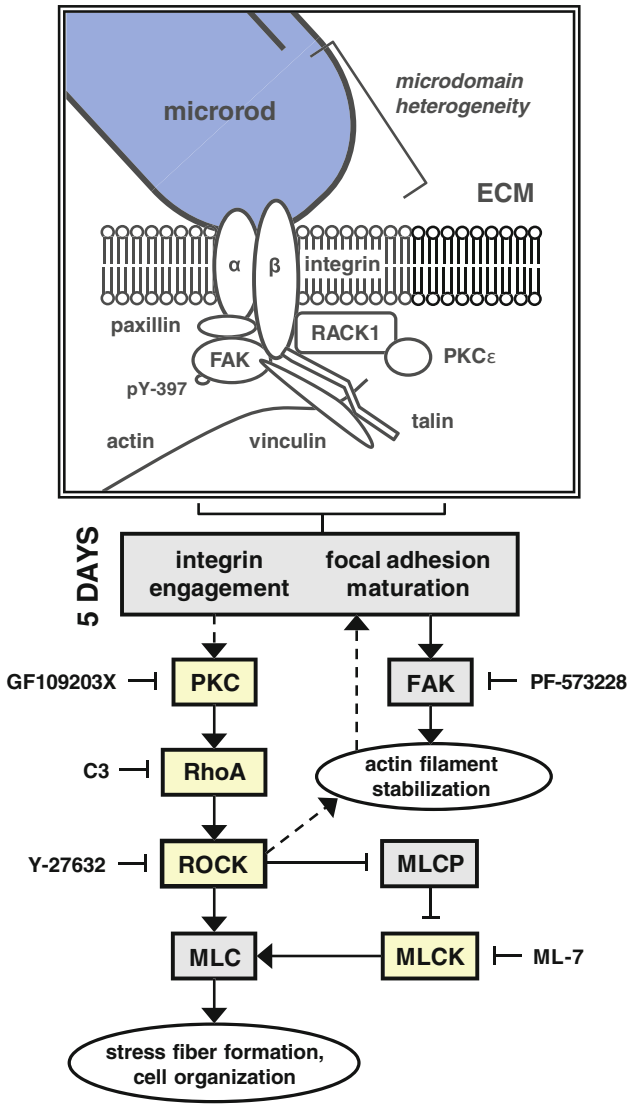

Fig. 7 Possible mechanism of microrod-affected mechanics in cardiac myocytes. The schematic depicts the various signaling molecules that have demonstrated an involvement in the recognition of microrods, based on measurements of axial displacement in spontaneously beating myocytes. Microrods in 3D gels introduce local heterogeneity, which ultimately elicits differences in maximum displacement and shortening velocity by 5 days in culture. While focal adhesions are likely to mature soon after cell seeding, it is the maintenance of PKC and RhoA/ROCK signaling that appears to mediate the microrod-related changes in contractile behavior. As such, these changes were abrogated upon ≥24-h inhibition of RhoA, ROCK, MLCK, and PKC by C3 Transferase, Y-27632, ML-7, and GF109203X, respectively. However, targeting of active FAK kinase (identified by phosphorylation at tyrosine residue 397) from day 2 to day 5 with PF-573228 did not prevent the response to microrods. This suggests that the required activity of RhoA/ROCK is downstream of PKC but not FAK. Yet curiously, PKC is known to be regulated both upstream and downstream of FAK signaling (Ruwhof et al. 2001; Heidkamp et al. 2003). The major calcium-independent isoform of PKC in the heart, PKCε, has been shown to bind receptor for activated C-kinase-1 (RACK1), which concurrently associates with β-integrin subunits; the complex promotes integrin clustering and focal adhesion development (Mochly-Rosen et al. 1991; Besson et al. 2002). In the diagram, proteins in *boxes shaded yellow* had activities that were found to participate in the effects of microrods

cardiac myocyte contraction. Such heterogeneity, represented through a model system combining cardiac myocytes and stiff polymeric microrods in a soft gel matrix, appears to affect aspects of cell remodeling without acting as a resistive load for muscle. When present, these microrod cues have a certain dependence on RhoA/ROCK and PKC signaling to carry out changes in cell size and contractility. Understanding the physical cues that drive the ability of single myocytes to shorten, develop anisotropic tension, and ultimately pump as part of effective myocardial tissue can inform a number of tissue engineering approaches that are applicable to the intact heart.

Acknowledgments Many thanks to students Waylon Smart and Santos Marrero for their help in digitizing captured cardiac myocyte displacements under the supervision of Dr. Elisa Budyn. Additional thanks to Kathleen Broughton for performing independent validations of image analyses. This work was supported by NIH grants T32 HL007692, PO1 HL62426, and RO1 HL090523. Additional counsel was provided by the Chicago Biomedical Consortium with support from the Searle Funds at the Chicago Community Trust.

References

Ayala P, Lopez JI, Desai TA (2010) Microtopographical Cues in 3D attenuate fibrotic phenotype and extracellular matrix deposition: implications for tissue regeneration. Tissue Eng Part A 16(8):2519–2527

Ayala P, Desai TA (2011) Integrin $\alpha 3$ blockade enhances microtopographical down-regulation of α-smooth muscle actin: role of microtopography in ECM regulation. Integr Biol (Camb) 3(7): 733–741

Bakunts K, Gillum N, Karabekian Z, Sarvazyan N (2008) Formation of cardiac fibers in Matrigel matrix. Biotechniques 44(3):341–348

Besson A, Wilson TL, Yong VW (2002) The anchoring protein RACK1 links protein kinase Cepsilon to integrin beta chains. Requirements for adhesion and motility. J Biol Chem 277(24):22073–22084

Bian W, Liau B, Badie N, Bursac N (2009) Mesoscopic hydrogel molding to control the 3D geometry of bioartificial muscle tissues. Nat Protoc 4(10):1522–1534

Bischofs IB, Schwarz US (2003) Cell organization in soft media due to active mechanosensing. Proc Natl Acad Sci USA 100(16):9274–9279

Bray MA, Sheehy SP, Parker KK (2008) Sarcomere alignment is regulated by myocyte shape. Cell Motil Cytoskeleton 65(8):641–651

Budyn E, Hoc T (2010) Analysis of micro fracture in human haversian cortical bone under transverse tension using extended physical imaging. Int J Numer Meth Eng 82(8):940–965

Chopra A, Tabdanov E, Patel H, Janmey PA, Kresh JY (2011) Cardiac myocyte remodeling mediated by N-cadherin-dependent mechanosensing. Am J Physiol Heart Circ Physiol 300(4): H1252–H1266

Collins JM, Ayala P, Desai TA, Russell B (2010) Three-dimensional culture with stiff microstructures increases proliferation and slows osteogenic differentiation of human mesenchymal stem cells. Small 6(3):355–360

Cukierman E, Pankov R, Stevens DR, Yamada KM (2001) Taking cell-matrix adhesions to the third dimension. Science 294(5547):1708–1712

Curtis MW, Sharma S, Desai TA, Russell B (2010) Hypertrophy, gene expression, and beating of neonatal cardiac myocytes are affected by microdomain heterogeneity in 3D. Biomed Microdev 12(6):1073–1085

DiMichele LA, Hakim ZS, Sayers RL, Rojas M, Schwartz RJ, Mack CP, Taylor JM (2009) Transient expression of FRNK reveals stage-specific requirement for focal adhesion kinase activity in cardiac growth. Circ Res 104(10):1201–1208

Doumalin P, Bornert M, Caldemaison D (1999) Microextensometry by image correlation applied to micromechanical studies using the scanning electron microscopy. In: Proceedings of the international conference on advanced technology in experimental mechanics, Japan Society of Experimental Engineering, pp 81–86

Doumalin P (2000) Microextensométrie locale par corrélation d'images numériques. Dissertation, Ecole Polytechnique

Doumalin P, Bornert M, Crepin J (2003) Characterization of the strain distribution in heterogeneous materials. Mecan Ind 6:607–617

Eble DM, Qi M, Waldschmidt S, Lucchesi PA, Byron KL, Samarel AM (1998) Contractile activity is required for sarcomeric assembly in phenylephrine-induced cardiac myocyte hypertrophy. Am J Physiol 274(5 Pt 1):C1226–C1237

Engler AJ, Carag-Krieger C, Johnson CP, Raab M, Tang HY, Speicher DW, Sanger JW, Sanger JM, Discher DE (2008) Embryonic cardiomyocytes beat best on a matrix with heart-like elasticity: scar-like rigidity inhibits beating. J Cell Sci 121(Pt 22):3794–3802

Evans HJ, Sweet JK, Price RL, Yost M, Goodwin RL (2003) Novel 3D culture system for study of cardiac myocyte development. Am J Physiol Heart Circ Physiol 285(2):H570–H578

Feng Z, Matsumoto T, Nakamura T (2003) Measurements of the mechanical properties of contracted collagen gels populated with rat fibroblasts or cardiomyocytes. J Artif Organs 6(3):192–196

Frey N, Olson EN (2003) Cardiac hypertrophy: the good, the bad, and the ugly. Annu Rev Physiol 65(1):45–79

Geisse NA, Sheehy SP, Parker KK (2009) Control of myocyte remodeling in vitro with engineered substrates. In Vitro Cell Dev Biol Anim 45(7):343–350

Geuzaine C, Remacle JF (2009) Gmsh: a three-dimensional finite element mesh generator with built-in pre- and post-processing facilities. Int J Numer Methods Eng 79(11):1309–1331

Goldyn AM, Rioja BA, Spatz JP, Ballestrem C, Kemkemer R (2009) Force-induced cell polarisation is linked to RhoA-driven microtubule-independent focal-adhesion sliding. J Cell Sci 122 (Pt 20):3644–3651

Gopalan SM, Flaim C, Bhatia SN, Hoshijima M, Knoell R, Chien KR, Omens JH, McCulloch AD (2003) Anisotropic stretch-induced hypertrophy in neonatal ventricular myocytes micropatterned on deformable elastomers. Biotechnol Bioeng 81(5):578–587

Grinnell F. (2000) Fibroblast-collagen-matrix contraction: growth-factor signalling and mechanical loading. Trends Cell Biol 10(9): 362–365

Grosberg A, Kuo PL, Guo CL, Geisse NA, Bray MA, Adams WJ, Sheehy SP, Parker KK (2011) Self-organization of muscle cell structure and function. PLoS Comput Biol 7(2):e1001088

Hartman TJ, Martin JL, Solaro RJ, Samarel AM, Russell B (2009) CapZ dynamics are altered by endothelin-1 and phenylephrine via PIP2 and PKC-dependent mechanisms. AJP Cell 296(5):C1034–C1039

Heidkamp MC, Bayer AL, Scully BT, Eble DM, Samarel AM (2003) Activation of focal adhesion kinase by protein kinase C epsilon in neonatal rat ventricular myocytes. Am J Physiol Heart Circ Physiol 285(4):H1684–H1696

Isemura M, Mita T, Satoh K, Narumi K, Motomiya M (1991) Myosin light chain kinase inhibitors ML-7 and ML-9 inhibit mouse lung carcinoma cell attachment to the fibronectin substratum. Cell Biol Int Rep 15(10):965–972

Jacot JG, McCulloch AD, Omens JH (2008) Substrate stiffness affects the functional maturation of neonatal rat ventricular myocytes. Biophys J 95(7):3479–3487

Kajzar A, Cesa CM, Kirchgessner N, Hoffmann B, Merkel R (2008) Toward physiological conditions for cell analyses: forces of heart muscle cells suspended between elastic micropillars. Biophys J 94(5):1854–1866

Kamgoué A, Ohayon J, Usson Y, Riou L, Tracqui P (2009) Quantification of cardiomyocyte contraction based on image correlation analysis. Cytometry A 75(4):298–308

Karlon WJ, Hsu PP, Li S, Chien S, McCulloch AD, Omens JH (1999) Measurement of orientation and distribution of cellular alignment and cytoskeletal organization. Ann Biomed Eng 27(6):712–720

Kaunas R, Nguyen P, Usami S, Chien S (2005) Cooperative effects of Rho and mechanical stretch on stress fiber organization. Proc Natl Acad Sci USA 102(44):15895–15900

Liu WF, Chen CS (2007) Cellular and multicellular form and function. Adv Drug Deliv Rev 59(13):1319–1328

Miyamoto S, Del Re DP, Xiang SY, Zhao X, Florholmen G, Brown JH (2010) Revisited and revised: is RhoA always a villain in cardiac pathophysiology?. J Cardiovasc Transl Res 3(4):330–343

Mochly-Rosen D, Khaner H, Lopez J (1991) Identification of intracellular receptor proteins for activated protein kinase C. Proc Natl Acad Sci USA 88(9):3997–4000

Moorman AF, Vermeulen JL, Koban MU, Schwartz K, Lamers WH, Boheler KR (1995) Patterns of expression of sarcoplasmic reticulum Ca(2+)-ATPase and phospholamban MRNAs during rat heart development. Circ Res 76(1):616–625

Motlagh D, Hartman TJ, Desai TA, Russell B (2003) Microfabricated grooves recapitulate neonatal myocyte connexin43 and N-cadherin expression and localization. J Biomed Mater Res A 67(1):148–157

Motlagh D, Senyo SE, Desai TA, Russell B (2003) Microtextured substrata alter gene expression, protein localization and the shape of cardiac myocytes. Biomaterials 24(14):2463–2476

Norman JJ, Collins JM, Sharma S, Russell B, Desai TA (2008) Microrods in 3D biological gels affect cell proliferation. Tissue Eng Part A 14(3):379–390

Okada J, Sugiura S, Nishimura S, Hisada T (2005) Three-dimensional simulation of calcium waves and contraction in cardiomyocytes using the finite element method. Am J Physiol Cell Physiol 288(3):C510–C522

Otani H, Yoshioka K, Nishikawa H, Inagaki C, Nakamura T (2011) Involvement of protein kinase C and RhoA in protease-activated receptor 1-mediated F-actin reorganization and cell growth in rat cardiomyocytes. J Pharmacol Sci 115(2):135–143

Pan J, Singh US, Takahashi T, Oka Y, Palm-Leis A, Herbelin BS, Baker KM (2005) PKC mediates cyclic stretch-induced cardiac hypertrophy through Rho family GTPases and mitogen-activated protein kinases in cardiomyocytes. J Cell Physiol 202(2):536–553

Parker KK, Tan J, Chen CS, Tung L (2008) Myofibrillar architecture in engineered cardiac myocytes. Circ Res 103(4):340–342

Parrag IC, Zandstra PW, Woodhouse KA (2011) Fiber alignment and coculture with fibroblasts improves the differentiated phenotype of murine embryonic stem cell-derived cardiomyocytes for cardiac tissue engineering. Biotechnol Bioeng, doi:10.1002/bit.23353

Patel AA, Thakar RG, Chown M, Ayala P, Desai TA, Kumar S (2010) Biophysical mechanisms of single-cell interactions with microtopographical cues. Biomed Microdev 12(2):287–296

Pedersen JA, Swartz MA (2005) Mechanobiology in the third dimension. Ann Biomed Eng 33(11):1469–1490

Qin L, Huang J, Xiong C, Zhang Y, Fang J (2007) Dynamical stress characterization and energy evaluation of single cardiac myocyte actuating on flexible substrate. Biochem Biophys Res Commun 360(2):352–356

Ren J, Fang CX (2005) Small guanine nucleotide-binding protein Rho and myocardial function. Acta Pharmacol Sin 26(3):279–285

Ross RS, Borg TK (2001) Integrins and the myocardium. Circ Res 88(11):1112–1119

Ruwhof C, van Wamel JT, Noordzij LA, Aydin S, Harper JC, van der Laarse A (2001) Mechanical stress stimulates phospholipase C activity and intracellular calcium ion levels in neonatal rat cardiomyocytes. Cell Calcium 29(2):73–83

Samarel AM (2005) Costameres, focal adhesions, and cardiomyocyte mechanotransduction. Am J Physiol Heart Circ Physiol 289(6):H2291–H2301

Shapira-Schweitzer K, Seliktar D (2007) Matrix stiffness affects spontaneous contraction of cardiomyocytes cultured within a PEGylated fibrinogen biomaterial. Acta Biomater 3(1):33–41

Sharp WW, Simpson DG, Borg TK, Samarel AM, Terracio L (1997) Mechanical forces regulate focal adhesion and costamere assembly in cardiac myocytes. J Physiol 273(2 Pt 2):H546–H556

Simpson DG, Majeski M, Borg TK, Terracio L (1999) Regulation of cardiac myocyte protein turnover and myofibrillar structure in vitro by specific directions of stretch. Circ Res 85(10):e59–e69

Slack-Davis JK, Martin KH, Tilghman RW, Iwanicki M, Ung EJ, Autry C, Luzzio MJ, Cooper B, Kath JC, Roberts WG, Parsons JT (2007) Cellular characterization of a novel focal adhesion kinase inhibitor. J Biol Chem 282(20):14845–14852

Smith R (2007) Plot digitizer user's manual (version 2.4.1). http://plotdigitizer.sourceforge.net. Accessed 7 June 2010

Soonpaa MH, Kim KK, Pajak L, Franklin M, Field LJ (1996) Cardiomyocyte DNA synthesis and binucleation during murine development. Am J Physiol 271(5 Pt 2):H2183–H2189

Sutton MA, Cheng MQ, Peters WH, Chao YJ, McNeill SR (1986) Application of an optimized digital correlation method to planar deformation analysis. Image Vis Comput 4(1):143–150

Tiburcy M, Didié M, Boy O, Christalla P, Döker S, Naito H, Karikkineth BC, El-Armouche A, Grimm M, Nose M, Eschenhagen T, Zieseniss A, Katschinksi DM, Hamdani N, Linke WA, Yin X, Mayr M, Zimmermann WH (2011) Terminal differentiation, advanced organotypic maturation, and modeling of hypertrophic growth in engineered heart tissue. Circ Res 109(10):1105–1114

Torsoni AS, Marin TM, Velloso LA, Franchini KG (2005) RhoA/ROCK signaling is critical to FAK activation by cyclic stretch in cardiac myocytes. Am J Physiol Heart Circ Physiol 289(4):H1488–H1496

Toullec D, Pianetti P, Coste H, Bellevergue P, Grand-Perret T, Ajakane M, Baudet V, Boissin P, Boursier E, Loriolle F (1991) The bisindolylmaleimide GF 109203X is a potent and selective inhibitor of protein kinase C. J Biol Chem 266(24):15771–15781

Tracqui P, Ohayon J, Boudou T (2008) Theoretical analysis of the adaptive contractile behaviour of a single cardiomyocyte cultured on elastic substrates with varying stiffness. J Theor Biol 255(1):92–105

Uehata M, Ishizaki T, Satoh H, Ono T, Kawahara T, Morishita T, Tamakawa H, Yamagami K, Inui J, Maekawa M, Narumiya S (1997) Calcium sensitization of smooth muscle mediated by a Rho-associated protein kinase in hypertension. Nature 389(6654):990–994

Zhang J, Jin G, Ma S, Meng L (2003) Application of an improved subpixel registration algorithm on digital speckle correlation measurement. Opt Laser Technol 35:533–542

Zhao Y, Lim CC, Sawyer DB, Liao R, Zhang X (2007) Simultaneous orientation and cellular force measurements in adult cardiac myocytes using three-dimensional polymeric microrods. Cell Motil Cytoskeleton 64(9):718–725

Zhou JJ, Bian JS, Pei JM, Wu S, Li HY, Wong TM (2002) Role of protein kinase C-epsilon in the development of kappa-opioid receptor tolerance to U50,488H in rat ventricular myocytes. Br J Pharmacol 135(7):1675–1684